Theoretical Prediction of Shear Strength Evolution in Steel Fibre Reinforced Concrete Beams without Stirrups

By

Timothy NYOMBOI[1], Hiroshi MATSUDA[2], Ryu HIRAYAMA[3], and Hiroshi NISHIDA[4],

Recent research has shown that steel fibres significantly increase the shear capacity and ductility in reinforced concrete (RC) beams. Utilization of this structural capacity in RC beams has however, been limited by lack of design guidelines. Conventional methods applied in normal design are not applicable in this case. Furthermore there exists no unified expression for the complete characterization of shear strength and ductility in beams. Fundamentally, steel fibres contribution should be considered based on stress transfer mechanism, augmented by concrete and dowel action of the main reinforcements in a unified manner. This paper proposes a unified analytical model in which the complete behavior of steel fibre reinforced concrete beams is characterized. Verification of the model was found to be in agreement with the experimental results tested by the authors. Non linear behavior as well as increase in strength observed in the fibrous beams was predicted well.

Key words**:** *Steel fibres concrete, Theoretical model, Shear Strength, Electronic speckle interferiometry (ESPI)*

1. Introduction

Current application of steel fibres in concrete structures is found in areas where improved crack control, fatigue resistance, earthquakes resistance, impact loads and slope stabilizations (using fibre short-Crete) is necessary. Many researchers [1-5, 7] have also established that use of steel fibres in concrete, lead to increased shear capacity and ductility in reinforced concrete. The knowledge of the behavior and ability to predict the same is therefore paramount to the development of guidelines for design applications and utilization of the aforementioned benefit in structural systems such as beams. Researchers have acknowledged that shear phenomenon is a complex and difficult property to predict [3, 4, and 6]. A lot has been done on the computation of the ultimate shear capacity mainly with the use of simplified models and experimental data [2, 3, 5, and 7]. However, there is no much information on a rational method for the prediction of the actual contribution by the steel fibres concrete composite and the dowel action of the main reinforcements. In this paper a simplified strain ratio based analytical model for the prediction of complete evolution of shear strength in steel fibre reinforced concrete (s.f.r.c) beams failing in shear is proposed. The shear resistance due to steel fibre reinforced concrete and the dowel action of the main reinforcements have all been considered based on equilibrium of forces and the stress transfer mechanisms.

2. Shear Strength analytical model derivations

In the derivation of the analytical model, the expressions for the various forces acting to resist the shear stress were first determined as outlined in the subsequent sections. Finally equilibrium conditions between the internal forces and the applied external load were evaluated to arrive at a unified predictive relation. The following assumptions were considered.

(i) Plane sections remain plane
(ii) Failure is predominantly by shear
(iii) Shear crack occurs at an angle of 45 degrees
(iv) Concrete is brittle while steel fibres are elastic,
(v) Fibre ultimately pull out from one side

平成20 年 6 月27 日受理

[1] Graduate school, Department of Structural Engineering
[2] Prof. Department of structural Engineering
[3, 4] Department of structural Engineering

(vi) Re bars dowel action contribute to shear strength

The geometry and loading conditions used in the derivation are as indicated in Fig.1

Due to symmetry, only half of the geometry in Fig.1 (portion *JKLM*) has been considered and its sheared profile analyzed. Based on Gere and Timonshenko`s shear deformations in a beam [8], the cracked sheared profile of portion *JKLM* has been assumed to correspond to the profile shown in Fig.2.0(a) while the stress, strain and crack opening diagrams along the crack path have been considered to be as shown in Fig.3.(a), (b), (c)(d).

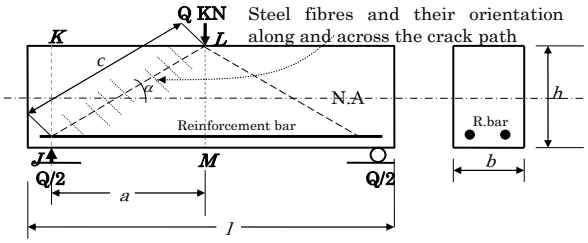

Fig.1 Basic details of the model beam

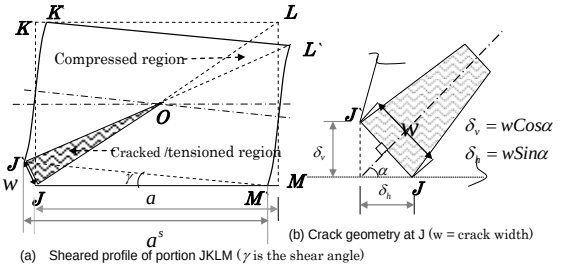

Fig.2 Cracked sheared profile of portion JKLM and details at joint J

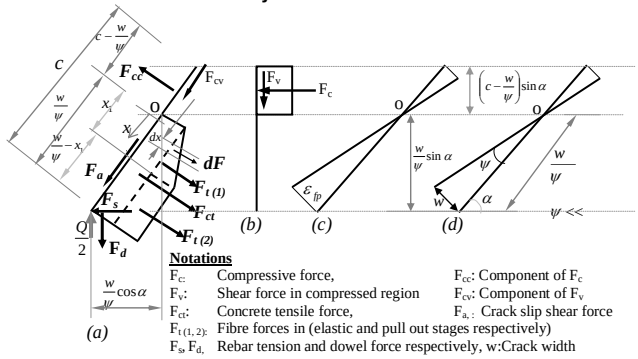

Fig. 3 simplified stress/force (*a,b*), strain (*c*) and crack rotation (*d*) diagrams

2.1 Forces acting to resist the shear

(1) Compressive force F_{cc} and Tensile force F_{ct}

From the geometry in Fig.1 and the stress profile (Fig.3a), the expression for the concrete compressive and tensile forces along the idealised crack path can be determined. The compressive force component is obtained from the following relation:

$$F_{cc} = \frac{F_c}{\sin\alpha} = \sigma_c b\left(c - \frac{w}{\psi}\right) \quad (1)$$

Where b and w are the beam and crack widths respectively, while ψ is the angle of crack rotation.

As idealized in Fig.3a, it is assumed that the concrete possess some minimal tensile strength. The resistive tensile force from the concrete is expressed as;

$$F_{ct} = \sigma_{ct} b\left(\frac{w}{\psi}\right) \quad (2)$$

Where σ_{ct} = the tensile strength of plain concrete

(2) Shear forces in compressed and cracked region

Determination of the concrete and crack-slip shearing forces **(**F_a and F_{cv}**)** in the compressed region and cracked region respectively, are considered in a unified manner under equilibrium analysis of all the forces (see section 2.2).

(3) Fibre tensile forces $F_{t\,(1)}$ and $F_{t\,(2)}$

In order to determine the expression for the steel fibre tensile forces $F_{t\,(1)}$ and $F_{t\,(2)}$ as shown in Fig 3(a), expressions for the average normal fiber force and strain is first established.

Average normal fibre force and pull out strain

The derivations are made by considering an infinitesimal force ***dF*** as shown in Fig 3(a) and orientation of the fibres across a shear crack, Fig.4

In the derivation, two regimes are considered as illustrated by the stress diagram in Fig.3 (a). These are;

-Elastic range (fibers elastically strain) $0 \le x \le x_1$

-Pull out range （fibers pulling out ） $x_1 \le x \le \frac{w}{\psi}$

Elastic Range

The force per fibre crossing the crack at right angles in the elastic range is determined as ;

$$F_f = E_f A_f \frac{w}{l_f} = E_f A_f \frac{x\psi}{l_f} \quad (3)$$

Where, A_f, E_f and ε_f are the area, elastic modulus, strain and fibre length, respectively.

From Fig.3 (d), the crack width w at any distance x is obtained $w = x\tan\psi \cong x\psi$ where ψ is small. Thus eq. 3 becomes

$$F_f = E_f A_f \frac{w}{l_f} = E_f A_f \frac{x\psi}{l_f} \quad (\text{Where } l_f = \text{the}) \quad (4)$$

The fibres are randomly distributed (Fig.4). The average normal fibre force is determined as;

$$F_{fN}^{e} = \frac{1}{\pi}\int_0^{\pi} F_f \sin\theta d\theta \quad (5)$$

Substituting for the force per fibre from eq.4 and integrating;

$$F_{fN}^{e} = \frac{2}{\pi} E_f A_f \frac{x\psi}{l_f} \quad (6)$$

Pull out range

The average normal fibre force in the pull out range is determined as

$$F_{fN}^{p} = \frac{2}{\pi} E_f A_f \varepsilon_{fp} \quad (7)$$

Where $\varepsilon_{fp} = \frac{x\psi}{l_f}$ is the fibre strain, equivalent to the effective pullout strain value after cracking.

Fibre pull-out strain ε_{fp}

The fibre pull out strain is a function of the bond stress τ_b and the fibre aspect ratio A_r. To derive an expression for the pull out strain, an arbitrarily fibre pull out mechanism as shown in Fig.5 is considered. The equilibrium of force between the concrete matrix and a fibre under tension will be;

$$A_f \sigma_{ft} = A_c \sigma_{ct} - A_f \sigma_{fc} \quad (8)$$

Where A_f and A_c are the fibre and concrete areas respectively while σ_{ft} and σ_{tc} are the fibre and concrete stresses respectively. Assuming that the effect of the fibre compression force is negligible;

$$A_f \sigma_{ft} = A_c \sigma_{ct} \quad (9)$$

Equilibrium of forces at the fibre-concrete interface is expressed as

$$A_c \sigma_{ct} = \tau_b \pi d_f l_f \quad (10)$$

For fibre pull out to occur, the force in the fibre should exceed the interfacial shear force. This can be expressed by combining eq.s 9 and 10 as;

$$A_f \sigma_{ft} \geq A_c \sigma_{ct} \geq \tau_b \pi d_f l_f$$

$$\therefore \quad A_f E_f \varepsilon_{fp} \geq \tau_b \pi d_f l_f \quad (11)$$

$$\varepsilon_{fp} = \frac{\tau_b \pi d_f l_f}{A_f E_f} \quad (12)$$

Experimental investigations have shown that the net fibre pull out length is equal to $l_f/4$[7], thus eq. 12 can be re-written as

$$\varepsilon_{fp} = \frac{\tau_b A_r}{E_f} \text{ or } \varepsilon_{fp} = \frac{\sigma_\tau}{E_f} \quad (13)$$

Where $A_r = \frac{l_f}{d_f}$ = fibre aspect ratio

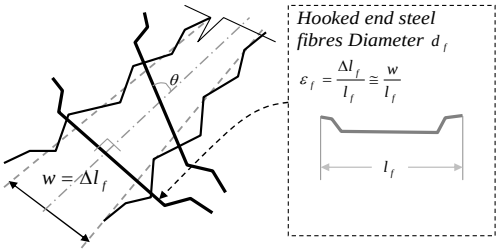

Fig.4 Fibre behavior across a shear crack

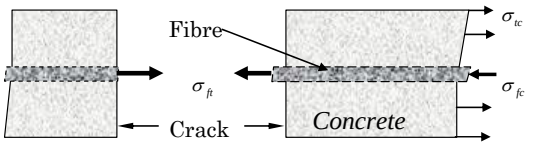

Fig. 5 Fibre pull-out equilibrium mechanism

(2) Force $F_{t\,(1)}$

Referring to the stress diagram in Fig.3a, the tensile force carried by the fibres during the elastic stage is determined as follows;

$$F_{t(1)} = \int_0^{x_1} dF \qquad \text{Where } dF = N_f \times F_{fN}^{e} \quad (14)$$

N_f = Number of fibres cross the crack

The number of fibres can be derived based on the fraction of fibres V_f crossing the crack as follows;

$$V_f = \frac{N_f A_f}{A_{sc}} = \frac{N_f A_f}{bdx}$$

Where A_f is cross sectional area of a single fibre

$$\therefore \quad N_f = \frac{V_f b dx}{A_f} \quad (15)$$

Substituting for F_{fN}^{e} from eq. 6 and N_f from eq. 15 above, the relation for $F_{t(1)}$ in eq. 14 is obtained as;

$$F_{t(1)} = \frac{2E_f b V_f \psi}{\pi l_f} \int_0^{x_1} x dx = \frac{E_f b V_f \psi x_1^2}{\pi l_f} \quad (16)$$

Assuming that at pull out stage, the strain in the fibre is equal to the pull out strain;

$\varepsilon_f = \varepsilon_{fp}$. From Fig 3a,

$x = x_1 \cong \frac{w}{\psi}$, and from Fig.4, $\varepsilon_f = \frac{\Delta l_f}{l_f} \cong \frac{w}{l_f}$

$$w = \Delta l_f = \varepsilon_f l_f, \text{thus } x_1 = \frac{\varepsilon_{fp} l_f}{\psi} \quad (17)$$

Where Δl_f = fibre pull-out displacement change corresponding to the increase in the crack width. Substituting for x_1 in eq. 16 from eq. 17, the force $F_{t(1)}$ is expressed as:

$$F_{t(1)} = \frac{E_f V_f b \varepsilon_{fp}^2 l_f}{\pi \psi} \quad (18)$$

With $K_1 = \frac{E_f V_f \varepsilon_{fp}}{\pi}$ (19)

eq. 18 can be re –written as

$$F_{t(1)} = \frac{K_1 b \varepsilon_{fp} l_f}{\psi} \quad (20)$$

(3) Force $F_{t(2)}$

Similarly from Fig.3, eq. 7 and 15, the expression for the pull out tensile force carried by the steel fibres is obtained as;

$$F_{t(2)} = F_{fN}^{p} N_f = \frac{2}{\pi} E_f \varepsilon_{fp} V_f b \left(\frac{w}{\psi} - x_1 \right) \quad (21)$$

Noting that $K_1 = \frac{E_f V_f \varepsilon_{fp}}{\pi}$ from eq. 20 and

$x_1 = \frac{\varepsilon_{fp} l_f}{\psi}$ From eq. 17 Eq. 21 is re-written as

$$F_{t(2)} = 2K_1 b \left(\frac{w}{\psi} - \frac{\varepsilon_{fp} l_f}{\psi} \right) \quad (22)$$

(4) Dowel Force F_d

The expression for the dowel force F_d has been derived based on dowel bearing mechanism in concrete road pavements [9]. It is assumed that the relative shear displacement between the crack faces is in tandem with that of the reinforcement bar as shown in Fig 6. The dowel load is transferred to the supporting concrete across the crack through bearing and the interface bond between concrete and the anchored part of the re-bar. Equations applied on dowel bars on concrete road pavements [9, 10] are applied in this study. Where ;

$$\sigma_b = k y_d \quad (23)$$

Where σ_b = bearing stress

y_d = deflection of the dowel bar (mm)

k = modulus of dowel support (N/mm^2),

The value of modulus of dowel support is estimated from that suggested by Frigberg [10].

$$k = 6895 \text{ or } 0.25\sqrt{E_c} \quad (24)$$

Referring to Fig.6 and applying eq.23 in the derivation of dowel force F_d,

$$F_d = \sigma_b d_b = k y_d d_b \quad (25)$$

Re-writing eq.25 in terms of the area of the reinforcement bar and substituting for $y_d = \frac{\delta_v}{2} = \frac{w\cos\alpha}{2}$ from ig.6, Fig.2b, then

$$y_d = \frac{\delta_v}{2} = \frac{w\cos\alpha}{2} \quad (26)$$

$$F_d = kw \cos\alpha \sqrt{\frac{A_s}{\pi}} \quad (27)$$

However, from the geometry of Fig.2a the shear displacement in relation to the shear angle γ (equal to shear strain) is determined as;

$$\delta_v = w\cos\alpha = a\tan\gamma \cong a\gamma \quad (\gamma \text{ is small}) \quad (28)$$

$$a = c\cos\alpha \quad \text{(From Fig 1)} \quad (29)$$

Combination of eq. 28 and 29 yields the expression for the general crack width as;

$$w = c\gamma \quad (30)$$

Where, c = the general length of the crack path

The crack width is expressed from eq.30 in terms of fibre pull out strain and initial yield shear strain γ_y as;

$$w = c\gamma \quad c\gamma_y \frac{\gamma}{\gamma_y} = \varepsilon_{fp} l_f \frac{\gamma}{\gamma_y} \quad (31)$$

Where $c\gamma_y = \varepsilon_{fp} l_f$ is the initial yield crack width 32

The actual net fibre pull out length is given as $0.25l_f$ [7], however this length is reduced during gradual pull out of the fibre. Thus the remaining effective length expressed in terms of the yield shear strain ratio after substitution of (*cy)* from 33 becomes

$$l_f^{ef} = l_f - w = 0.25 l_f \left(1 - 4\varepsilon_{fp} \frac{\gamma}{\gamma_y} \right) \quad (33)$$

Re-writing the term (*w)* in eq 27 in terms of eq. 33 the expression for the dowel force will be;

$$F_d = k\varepsilon_{fp} l_f^{ef} \frac{\gamma}{\gamma_y} \cos\alpha \sqrt{\frac{A_s}{\pi}} \quad (34)$$

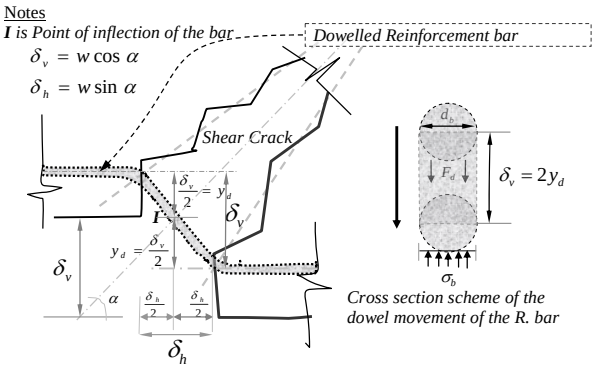

Fig. 6 Relative deflections of Reinforcement bar and the crack faces

(5) Bar Tensile Force F_s

The tensile force acting on the re bar can be assessed in a similar manner as that of the fibre. An effective pull out length from the shortest anchored side from the crack face is assumed. The tensile force

acting on the re bar is determined as;

$$F_s = A_s\sigma_s = A_s E_s \varepsilon_{sp} \quad (35)$$

Where A_s, E_s σ_s are the area, elastic modulus and stress of the re bar.

Substituting for strain from eq.12, with replacement of fibre parameters with those of the bar reinforcement, then

$$F_s = 2\pi\tau_b l_a^{ef}\sqrt{\frac{A_s}{\pi}} \quad (36)$$

Where τ_b = Bond shear strength and

$$l_a^{ef} = l_a - w = l_a - \varepsilon_{fp} l_f \frac{\gamma}{\gamma_y}$$

2.2 Shear Strength Predictive Eq.

The overall shear strength predictive relation is derived based on the equilibrium of external and internal forces previously derived in section 2.1.

(1)Horizontal Equilibrium

$$\left(F_{t(1)} + F_{t(2)} - F_c + F_{ct}\right)\sin\alpha + F_s = (F_{cv} + F_a)\cos\alpha$$

$$F_{cv} + F_a = \left(F_{t(1)} + F_{t(2)} - F_c + F_{ct}\right)\frac{\sin\alpha}{\cos\alpha} + \frac{F_s}{\cos\alpha} \quad (37)$$

(2) Vertical Equilibrium

$$\frac{Q}{2} - \left(F_{t(1)} + F_{t(2)} - F_c + F_{ct}\right)\cos\alpha - (F_{cv} + F_a)\sin\alpha - F_d = 0 \quad (38)$$

From eq.37, $(F_{cv}+F_a)$ is substituted in eq. 38 to obtain;

$$\left(F_{t(1)} + F_{t(2)} - F_c + F_{ct}\right) + F_s\sin\alpha + F_d\cos\alpha = \frac{Q}{2}\cos\alpha \quad (39)$$

(3) Moment equilibrium about point O (Fig 3, 2)

Moment equilibrium about the point of shear crack rotation O (Fig.3);

$$\frac{Q}{2}\frac{w}{\psi}\cos\alpha - \frac{1}{2}F_c\left(c - \frac{w}{\psi}\right) - F_{t(2)}\left\{x_1 + \frac{1}{2}\left(\frac{w}{\psi} - x_1\right)\right\} - \frac{2}{3}F_{t(1)}x_1 - F_d\frac{w}{\psi}\cos\alpha - F_s\frac{w}{\psi}\sin\alpha - \frac{1}{2}F_{ct}\frac{w}{\psi} = 0$$

Force relation given in eq.s 1, 2 20, 22, 34 and 36 respectively, are substituted in the above.

$$\frac{Q}{2b}\frac{w}{\psi}\cos\alpha - \frac{\sigma_c}{2}\left(c^2 - 2c\frac{w}{\psi} + \left(\frac{w}{\psi}\right)^2\right) + \frac{1}{3}k_1\left(\frac{\varepsilon_{fp}l_f}{w}\right)^2\left(\frac{w}{\psi}\right)^2 - k_1\left(\frac{w}{\psi}\right)^2 - \frac{F_d}{b}\frac{w}{\psi}\cos\alpha - \frac{F_s}{b}\frac{w}{\psi}\sin\alpha - \frac{\sigma_{ct}}{2}\left(\frac{w}{\psi}\right)^2 = 0$$

Reducing further to

$$\left(\frac{w}{\psi}\right)^2\left\{-\frac{\sigma_c}{2} + \frac{1}{3}K_1\left(\frac{\varepsilon_{fp}l_f}{w}\right)^2 - K_1 - \frac{\sigma_{tc}}{2}\right\} + \frac{w}{\psi}\{Q_1 + c\sigma_c - F_1 - F_2\} = \frac{c^2\sigma_c}{2} \quad (40)$$

$$Q_1 = \frac{Q}{2b}\cos\alpha,\quad F_1 = \frac{F_d}{b}\cos\alpha,\quad F_2 = \frac{F_s}{b}\sin\alpha \quad (41)$$

The expression for $\frac{w}{\psi}$ is obtained from eq. 38 as:

$$\frac{w}{\psi} = \frac{Q_1 + c\sigma_c - F_1 - F_2}{2k_1 - K_1\frac{\varepsilon_{fp}l_f}{w} + \sigma_c + \sigma_{ct}} \quad (42)$$

Substituting eq.38 and determining the approximate solution, eq.41 becomes;

$$Q = {}_1\frac{cK_1}{3}\left\{3 - \left(\frac{\varepsilon_{fp}l_f}{w}\right)^2 - \left[\frac{k_1}{\sigma_c}\left(2 - \frac{\varepsilon_{fp}l_f}{w}\right) + \frac{\sigma_{ct}}{\sigma_c}\right]\right\} \left\{\left[\frac{3\sigma_{ct}}{2K_1} + 3 + \left(\frac{\varepsilon_{fp}l_f}{w}\right)^2 - 3\frac{\varepsilon_{fp}l_f}{w}\right]\right\} + \frac{c\sigma_{ct}}{2} + F_1 + F_2 \quad (43)$$

Substitute for Q_1, F_1, F_2 from eq.41 and with $c = a/\cos\alpha$ (Fig.1). From the shear span to depth ratio relation, $a = d\beta$. Thus eq.43 becomes;

$$\frac{Q}{2} = \frac{db\beta K_1}{3\cos^2\alpha}\left\{3 + \left(\frac{\varepsilon_{fp}l_f}{w}\right)^2 - \left[\frac{k_1}{\sigma_c}\left(2 - \frac{\varepsilon_{fp}l_f}{w}\right) + \frac{\sigma_{ct}}{\sigma_c}\left[\frac{3\sigma_{ct}}{2k_1} + 3 + \left(\frac{\varepsilon_{fp}l_f}{w}\right)^2 - 3\frac{\varepsilon_{fp}l_f}{w}\right]\right\} + \frac{db\beta\sigma_{ct}}{2\cos^2\alpha} + F_d + F_s Tan\alpha \quad (44)$$

To account for the influence of the shear span to depth ratio in shear, eq.44 is re written as follows

$$\frac{Q}{2} = \frac{db\beta^2 K_1}{3\beta\cos^2\alpha}\left\{3 + \left(\frac{\varepsilon_{fp}l_f}{w}\right)^2 - \left[\frac{k_1}{\sigma_c}\left(2 - \frac{\varepsilon_{fp}l_f}{w}\right) + \frac{\sigma_{ct}}{\sigma_c}\left[\frac{3\sigma_{ct}}{2k_1} + 3 + \left(\frac{\varepsilon_{fp}l_f}{w}\right)^2 - 3\frac{\varepsilon_{fp}l_f}{w}\right]\right\} + \frac{db\beta^2\sigma_{ct}}{2\beta\cos^2\alpha} + F_d + F_s Tan\alpha$$

Dividing by β^2, the relation for a factored shear load in which the shear span to depth ratio influence is accounted is obtained as

$$V = \frac{Q}{2\beta^2} = \frac{dbK_1}{3\beta\cos^2\alpha}\left\{3 + \left(\frac{\varepsilon_{fp}l_f}{w}\right)^2 - \left[\frac{k_1}{\sigma_c}\left(2 - \frac{\varepsilon_{fp}l_f}{w}\right) + \frac{\sigma_{ct}}{\sigma_c}\left[\frac{3\sigma_{ct}}{2k_1} + 3 + \left(\frac{\varepsilon_{fp}l_f}{w}\right)^2 - 3\frac{\varepsilon_{fp}l_f}{w}\right]\right\} + \frac{db\sigma_{ct}}{2\beta\cos^2\alpha} + \frac{1}{\beta^2}(F_d + F_s Tan\alpha) \quad (45)$$

Substitution for w, F_d and F_s from eqs.31, 34 and 36 respectively, with simplification of the dowel contribution part (last term), the shear strength equation (in Newton) is then given as;

$$V = \frac{dbK_1}{3\beta\cos^2\alpha}\left\{3 - \left(\frac{\gamma_y}{\gamma}\right)^2 - \left[\frac{k_1}{\sigma_c}\left(2 - \frac{\gamma_y}{\gamma}\right) + \frac{\sigma_{ct}}{\sigma_c}\right]\right\} \left\{\left[\frac{3\sigma_{ct}}{2k_1} + 3 + \left(\frac{\gamma_y}{\gamma}\right)^2 - 3\frac{\gamma_y}{\gamma}\right]\right\} + \frac{db\sigma_{ct}}{2\beta\cos^2\alpha} + \frac{1}{\beta^2}\sqrt{\frac{A_c\rho}{\pi}} \left(k\varepsilon_{fp}l_f^{ef}\frac{\gamma}{\gamma_y}\cos\alpha + 2\pi\tau_b l_a^{ef}\tan\alpha\right) \quad (46)$$

It can be seen that eq.46 follows the traditionally applied principle of superposition and can simply be written as

$$V = V_{fc} + V_c + V_d \quad (47)$$

In order to make evolution predictions, the shear strain ratio in eq.46 must be applied incrementally (ie $\frac{\gamma_y}{\gamma}$ =0, 1, 2, 3 etc) in the prediction analysis.

The yield shear strain is determined theoretically based on the relation given by Gere and Timoshenko [8], however since this is not the maximum value, the factor applied in the given equation has been assumed to be equal to 1.2.

$$\gamma_y = \frac{1.2 Q_y}{2 G A_c} \quad (48)$$

Where the yield shear load is at shear ratio of 1

$G = \frac{E_c}{2(1+\upsilon)}$, is the shear modulus ($N/mm^2$) (49)

A_c = Cross sectional area of the concrete beam

υ = Poisson ratio

2.3 Determination of deflections

Deflections at mid span of the beam are obtained by combination of moment-curvature relations [8] and moment-deflection relations [12]. The curvature ratio relationship in beams before and after cracking is given as follows [8]:

$$\frac{\kappa}{\kappa_y} = \frac{1}{\sqrt{3 - \frac{2M}{M_y}}} \quad (50)$$

Where $\kappa = \frac{1}{\rho}$ is the curvature in elastic bending and κ_y is curvature at yielding beyond which inelastic bending occurs, M is the general moment between the yield and plastic moment, respectively. That is $M_y \le M \le M_p$

Estimation of the mid span deflection due to elastic bending is obtained based on the relations given in [12]. Based the relations, elastic deflection in beam under bending is given as:

$$\delta_e = \xi l_e^2 \frac{1}{\rho} \quad (51)$$

Where $\xi = \frac{4\varphi^2 - 8\varphi + 1}{48\varphi}$ and $\varphi = a / l_e$

For small deflections, moment curvature relationship in elastic bending can be determined as

$\frac{1}{\rho} = \frac{M}{EI}$ noting that here $0 \le M \le M_y$ (52)

It is assumed in this study that at onset of yield, the elastic curvature limit is equal to yield curvature, therefore

. $\frac{1}{\rho} = \frac{1}{\rho_y} = \kappa_y$ (53)

Combination of eq.51 to 54 yields the relation for the determination of deflections (eq.54) from elastic to inelastic bending (after cracking). By inspection of eq.60, the curvature ratio range is found to be within a ratio not exceeding 1.73.

$$\delta_b = \frac{2\xi l_e M}{EI\left(3 - \left(\frac{\kappa_y}{\kappa}\right)^2\right)} \quad (54)$$

The deflections due to bending from eq. 54 are then added to shear deflections estimated from the relation between the shear strains and the shear displacement from eq. 28. Where the shear displacements are obtained as follows:

$$\begin{aligned} \delta_s &= a\gamma \\ &= a\gamma_y\left(\frac{\gamma}{\gamma_y}\right) \\ &= a\frac{1.2 Q_y}{2 G A_c}\left(\frac{\gamma_y}{\gamma}\right) \end{aligned} \quad (55)$$

The total deflections are then estimated as follows

$\delta_t = \delta_s + \delta_b$ (56)

3. Verification of shear strength formula eq. (46)

3.1 Basis of verification

Validity of the derived eq.46 was checked against experimental results obtained from a total of 12 test beams. Geometry and reinforcement details similar to those used in the experiments (Fig7) were used in the theoretical predictions. The tensile and compressive strengths applied were obtained from concrete cylinder tests; however the bond strength was estimated based on the value (*4.15*Mpa) proposed by Narayanan R, et al [2]. Other properties are as shown in Table1. Twelve simply supported beams under bending- shear (Fig.7) were tested in the experiments. Tests on the specimens were done using a 300kN capacity universal testing machine.

Controlled loading was applied on the specimens while the full field deformations (displacements) were monitored and recorded using a set of optical measurements equipment system (ESPI) comprising a Desk top computer (PC) and CCD camera (ESPI sensor) equipped with laser beam sensors as shown in Fig.8.

Table 1 Parameters applied in analysis

Reinforcements	l_f mm	30
	d_f mm	0.62
	A_r	60
	f_s (N/mm^2)	340
	f_{fy} (N/mm^2)	1000
	E_f (N/mm^2)	210000
	E_s (N/mm^2)	,, ,,
	Fibre content %	0, 0.5,1,1.5
Concrete	σ_c (N/mm^2)	38
	σ_{ct} (N/mm^2)	3.67
	E_c (N/mm^2)	31108
	υ	0.195
	k (N/mm^2)	6895

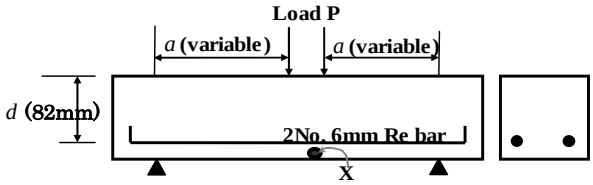

Fig.7 Test set up and measurement points

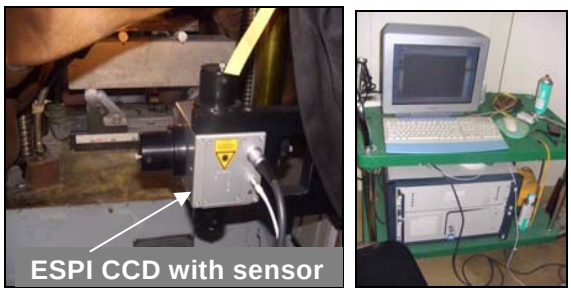

a) ESPI camera and specimen b) Processor

Fig. 8 Full filed optical equipment and set up

3.2 Verification results and Discussions

(1) Analytical predictions

Fig.9 shows the theoretical predictions from eq. (47) for fibrous beams. As depicted in these figures, the strength evolution behavior is approximately linear in the initial stages beyond which a non linear behavior is observed. Complete deformation behavior in which increase in the shear strength commensurate with the fibre content is predicted well. The reduction in shear strength with increase in the shear span to depth ratio, a phenomenon commonly observed in practice is also predicted well.

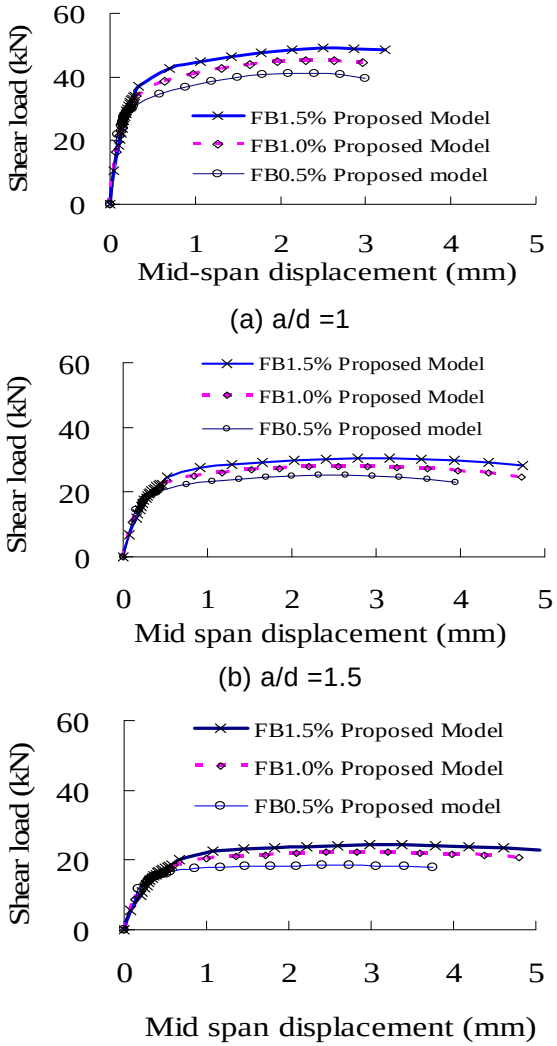

Fig. 9 Theoretical prediction eq. (46)

(2) Experimental and theoretical comparisons

Fig 10 shows comparisons between experimental and theoretical results. There is generally a very good correlation between the theoretical predictions and the experimental results. Both results also indicate an increase in strength in the fibrous beams over non fibrous beams. A decrease in the strength with increase in shear span depth ratio is also observed in both theoretical and experimental results. In Fig 10a, ductility representation after yield is observed to be limited in the ESPI results as compared with the theoretical predictions. This is because the failure was predominantly shear in which deformation after failure at mid span could not be detected well by the ESPI method due to presence of rigid displacement.

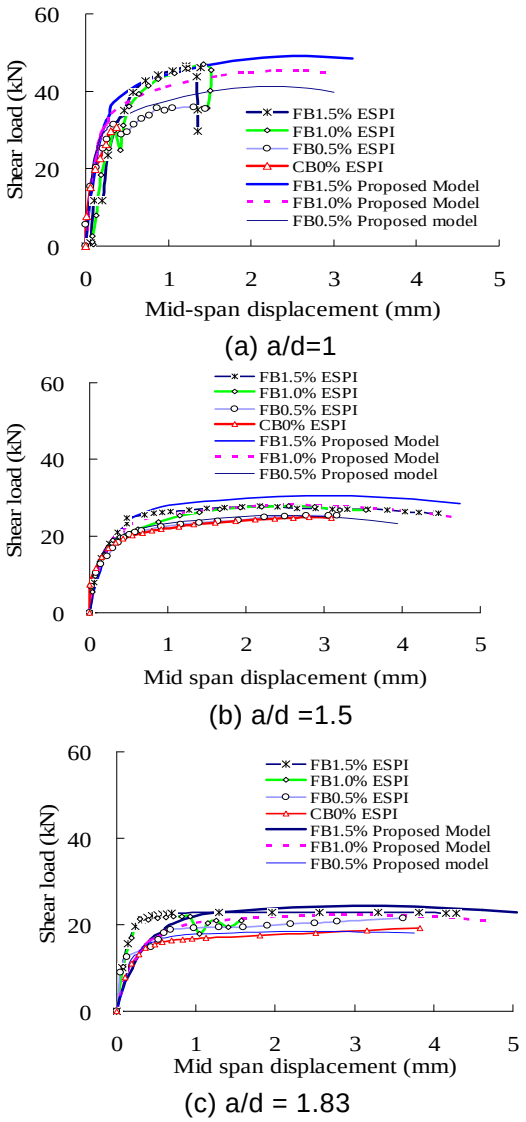

Fig.10 Experimental and theoretical comparison

4. Conclusions and Recommendations

The key assumptions made and validity of the derived theoretical model has been confirmed through comparison with experiments. The comparison showed that the model is consistently in agreement and conservative in all the cases considered. However, there is need for more experimental data to evaluate the model in detail particularly in prototype beams specimens.

Acknowledgement

Support from the Government of Japan through MEXT scholarship programme is highly appreciated.

Reference

1. Calogero C., Lidia L. M., Maurizio P., Effectiveness of stirrups and steel fibres as shear reinforcements. Elsevier, Cement and Concrete Composites 2004; 26: p.777 - 786.
2. Narayanan R, and Darwish, IYS. Use of steel fibres as shear reinforcement. ACI Structural Journal V.84, No.3, May – June 1987. p. 216-227.
3. Madhusudan Khuntia et al. Shear strength of Normal and High-strength fiber reinforced concrete beams without stirrups. ACI Structural Journal, V.96, No.2, March –April 1999. p. 282-290.
4. Shitote SM. Prediction of the Response of Fibre Reinforced Concrete Beams in Combined Shear and Flexure using the Compression Field Theory. Research Paper, Department of Structural Mechanics, Delft University of Technology. The Netherlands, 2000.
5. Nyomboi, T. et al., Stress Strain Relations for Steel fibre Reinforced Concrete Beams in Shear, Proceedings of International Conference on applied Mechanics, SACAM 2000, 11 – 13 January, Durban South Africa, pp. 355 -368. ISBN 1-86840-352-1.
6. Yasuhiko Sato, et al, Diagonal Tensile failure mechanism of Reinforced Concrete beams, Journal of Advanced Concrete Technology Vol. 2, No 3, pp 327-341, October 2004.
7. Lim D.H. and Oh B.H., Experimental and theoretical investigation on the shear of steel fibre reinforced concrete beams. Elsevier, Engineering structures, 1999; 21: p. 937-944
8. Gere and Timoshenko Mechanics of Materials. Second Edition (1989). p. 407 - 409.
9. Max LP et al. Assessment of Dowel Bar research. Iowa DOT Project HR-1080 CTRE project 00-93, Iowa State University. (August 2002). p. 52 – 58
10. Friberg BF. Design of Dowels in Transverse Joints of Concrete Pavements. Transactions, American Society of Civil Engineers; Vol. 105, No. 2081. 1940.
11. Stroud KA et al. Engineering Mathematics. Fifth edition, Palgrave Macmillan, 2001. p. 784-785.
12. Mosley W. H. and Bungey J.H., Reinforced concrete design, Fourth edition, Maccmillan Ltd, 1990, p. 119-127.